



Electrocatalysis Hot Paper

 How to cite: *Angew. Chem. Int. Ed.* **2023**, 62, e202218728

International Edition: doi.org/10.1002/anie.202218728

German Edition: doi.org/10.1002/ange.202218728

Alternating Metal-Ligand Coordination Improves Electrocatalytic CO₂ Reduction by a Mononuclear Ru Catalyst**

Hemlata Agarwala^{+,*}, Xiaoyu Chen⁺, Julien R. Lyonnet, Ben A. Johnson, Mårten Ahlquist,^{*} and Sascha Ott^{*}

Abstract: Molecular electrocatalysts for CO₂-to-CO conversion often operate at large overpotentials, due to the large barrier for C–O bond cleavage. Illustrated with ruthenium polypyridyl catalysts, we herein propose a mechanistic route that involves one metal center that acts as both Lewis base and Lewis acid at different stages of the catalytic cycle, by density functional theory in corroboration with experimental FTIR. The nucleophilic character of the Ru center manifests itself in the initial attack on CO₂ to form [Ru–CO₂]⁰, while its electrophilic character allows for the formation of a 5-membered metallacyclic intermediate, [Ru–CO₂CO₂]^{0,c}, by addition of a second CO₂ molecule and intramolecular cyclization. The calculated activation barrier for C–O bond cleavage via the metallacycle is decreased by 34.9 kcal mol^{–1} as compared to the non-cyclic adduct in the two electron reduced state of complex **1**. Such metallacyclic intermediates in electrocatalytic CO₂ reduction offer a new design feature that can be implemented consciously in future catalyst designs.

Introduction

Electrochemical reduction of CO₂ can assist in mitigating atmospheric CO₂ levels and offer scalable means to store

renewable electricity in energy dense compounds such as CO. Unfortunately, the electrochemical conversion of CO₂ to CO typically suffers from high overpotentials that impede efficient implementation.^[1–3] In molecular transition metal-based catalysts, three key steps have been identified as potential kinetic bottlenecks: 1) CO₂ binding to the catalyst that is accompanied by bending of linear CO₂, 2) cleavage of a C–O bond in the [metal–CO₂]ⁿ⁺ adduct and 3) CO dissociation from the catalyst. Of these three steps, the current report focuses mainly on C–O bond cleavage in molecular catalysts. Multiple electrochemical reduction steps to form a low-valent pre-catalytic state have been shown to facilitate this process, but these typically occur at more negative standard potentials, thus leading to high overpotentials.^[4–10] In nature, carbon monoxide dehydrogenase enzymes (CODH) can efficiently and reversibly convert CO to CO₂.^[11] In the active site of CODH from the anaerobic bacterium *C. hydrogenoformans*, there is a [Ni–4Fe–5S] cluster, called the C-cluster, which consists of a [Ni–3Fe–4S] cubane linked to a unique Fe site through a sulfide.^[12,13] In this cluster, Ni is the redox active center to which CO₂ binds. In close proximity is a redox inactive Fe^{III} Lewis acid that facilitates C–O cleavage by stabilizing the OH[–] group formed during the process.^[13] Efforts to mimic this function in artificial systems include the simple addition of Brønsted acids to enhance catalytic activity.^[4,5,7,10,14–36] Also, several metal complexes with intramolecular Brønsted

[*] Dr. H. Agarwala,⁺ J. R. Lyonnet, Dr. B. A. Johnson, Prof. Dr. S. Ott
 Department of Chemistry - Ångström Laboratories, Uppsala University
 Box 523, 75120 Uppsala (Sweden)
 E-mail: hemlataagarwala@gmail.com
 sascha.ott@kemi.uu.se
 Homepage: <https://ebt.cs.tum.de/team/?lang=en>
<https://www.kemi.uu.se/angstrom/research/synthetic-molecular-chemistry/research-groups/ott-group/>

Dr. H. Agarwala,⁺ Dr. B. A. Johnson
 Present address: Technical University of Munich (TUM), Campus Straubing for Biotechnology and Sustainability
 Uferstraße 53, 94315 Straubing (Germany)
 E-mail: hemlata.agarwala@tum.de

X. Chen,⁺ Prof. Dr. M. Ahlquist
 Department of Theoretical Chemistry and Biology, School of Engineering Sciences in Chemistry, Biotechnology and Health (CBH), KTH Royal Institute of Technology
 10691 Stockholm (Sweden)
 E-mail: ahlqui@kth.se

Homepage: <https://www.kth.se/profile/ahlqui/page/group?l=en>

J. R. Lyonnet
 Present address: Institute of Chemical Research of Catalonia (ICIQ), The Barcelona Institute of Science and Technology
 43007 Tarragona (Spain)

[†] These authors contributed equally to this work.

[**] A previous version of this manuscript has been deposited on a preprint server (<https://doi.org/10.26434/chemrxiv.14035625.v2>).

© 2023 The Authors. Angewandte Chemie International Edition published by Wiley-VCH GmbH. This is an open access article under the terms of the Creative Commons Attribution Non-Commercial NoDerivs License, which permits use and distribution in any medium, provided the original work is properly cited, the use is non-commercial and no modifications or adaptations are made.

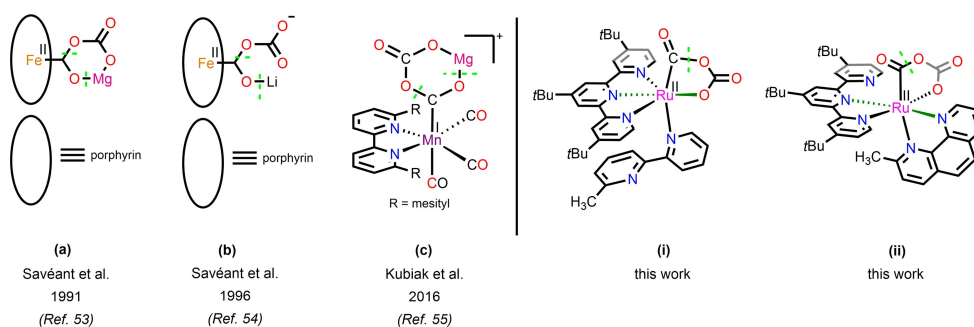


Figure 1. Representations of some transition metal-bound CO₂ adducts: (a–c) previously proposed,^[53–55] stabilized by Lewis acid (LA) cations like Mg²⁺ and Li⁺; (i and ii) investigated in the present work. The dashed green lines (---) indicate the scission of C–O and O–LA bonds in the subsequent step of the respective catalytic cycles.

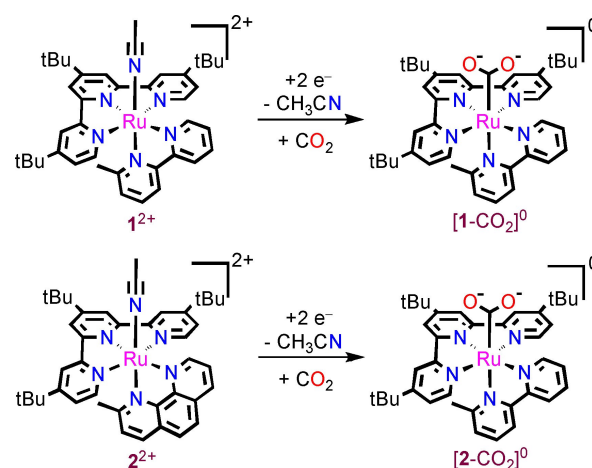
acidic groups positioned close to the reactive center have been shown to facilitate C–O cleavage.^[3,10,29,35,37–52]

Examples of catalytic rate enhancements for CO₂ electroreduction by Lewis acidic metal ions in molecular catalysts are comparatively rare.^[32,53–55] In some of these systems, cyclic intermediates that comprise the catalytic metal center, two molecules of CO₂ and an exogenous alkali or alkaline earth metal Lewis acid have been proposed^[53–55] (Figures 1a–1c); however, to the best of our knowledge, none was observed experimentally. It has been postulated that C–O cleavage from these cyclic intermediates is more facile compared to the systems without the additional Lewis acid. Herein, we report a unique pathway for C–O bond cleavage in the overall reductive disproportionation of CO₂ to CO and CO₃^{2–} that requires neither excessive catalyst reductions nor external Lewis acids. The mechanistic route involves *one* metal center that acts as both Lewis base and Lewis acid at different stages of the catalytic cycle. The pathway is enabled by the flexible ligation of polypyridine ligands that can liberate open coordination sites (Figures 1–(i) and 1(ii)).

Results and Discussion

The aforementioned mechanism is exemplified by two Ru-based catalysts, [Ru(*t*Bu₃tpy)(CH₃bpy)(CH₃CN)]²⁺ (**1**²⁺)^[56,57] and [Ru(*t*Bu₃tpy)(CH₃phen)(CH₃CN)]²⁺ (**2**²⁺) (Scheme 1; *t*Bu₃tpy = 4,4',4''-tri-*tert*-butyl-2,2':6',2''-terpyridine; CH₃bpy = 6-methyl-2,2'-bipyridine, CH₃phen = 2-methyl-1,10-phenanthroline) that differ in the bidentate ligand motif. The bidentate CH₃phen in **2**²⁺ is a structurally more rigid ligand due to the fusion of the two pyridine rings,^[58,59] rendering the ligand less prone to distortion, than CH₃bpy in **1**²⁺. The presence of the methyl group *ortho* to the nitrogen in the bidentate ligand is motivated by our previous finding that it labilizes the coordinated CH₃CN upon one-electron reduction of the complex.^[56]

Complexes **1**²⁺ and **2**²⁺ were prepared from Ru^{III}-(*t*Bu₃tpy)(Cl)₃ and the respective bidentate ligand by slight modifications of published procedures^[56] (see Experimental Section, and Figures S1 and S2, in Supporting Information).



Scheme 1. Pictorial representation of complexes **1**²⁺ and **2**²⁺, and their two-electron reduced CO₂ adducts [**1**-CO₂]⁰ and [**2**-CO₂]⁰, respectively.

As mentioned above, owing to the *ortho* methyl groups of the bidentate ligand, both complexes can liberate the CH₃CN ligand upon one-electron reduction.^[56] The coordinatively unsaturated intermediate acts as a Lewis base towards CO₂, ultimately leading to the two-electron reduced CO₂ adducts [**1**-CO₂]⁰ and [**2**-CO₂]⁰ (Scheme 1)^[56] which are the starting points of the present study.

The cyclic voltammograms (CVs) of complexes **1**²⁺ and **2**²⁺ show electrochemically reversible one-electron reductions under argon at –1.76 V and –1.77 V versus Fc^{+/0} respectively (Figure 2, Table S1), the cathodic peak potential being –1.81 V (versus Fc^{+/0}) for both.

The corresponding DFT calculated standard potentials of –1.84 V and –1.81 V versus Fc^{+/0} for **1**²⁺ and **2**²⁺ respectively, match well with the experimental values (See Computational details and Table S0 in Supporting Information). Linear variation of peak currents with the square root of the scan rate for the first reduction of **2**²⁺ under argon (Figure S3) reveals diffusion-controlled behavior, with the diffusion coefficient (*D*) being 8.11 × 10^{–6} cm² s^{–1} (details of calculation of *D* can be found under Figure S3 in Supporting Information).

Upon addition of CO₂ (0.28 M),^[60] the first reductions become irreversible with noticeable enhancement in catho-

$\text{CO}_2\text{CO}_2]{}^0$ (details of this calculation can be found under Figure S8). However, the 240 mV difference between the standard potential for the $[\mathbf{1}\text{-CO}_2\text{CO}_2]{}^{-1}/[\mathbf{1}\text{-CO}_2\text{CO}_2]{}^0$ couple and the applied potential, results in the concentration of $[\mathbf{1}\text{-CO}_2\text{CO}_2]{}^{-1}$ being four orders of magnitude lower than that of $[\mathbf{1}\text{-CO}_2\text{CO}_2]{}^0$ (calculations under Figure S8). Therefore, considering the cyclization to be a first order reaction, this difference in concentrations, combined with the relative rate constants of cyclization, leads to an overall apparent rate of formation of $[\mathbf{1}^{bp}\text{-CO}_2\text{CO}_2]{}^{-1,c}$ through $[\mathbf{1}^{bp}\text{-CO}_2\text{CO}_2]{}^0,c$ to be about 13 times faster than through $[\mathbf{1}\text{-CO}_2\text{CO}_2]{}^{-1}$ (calculations under Figure S8). This difference in the relative rates implies that both the competing pathways to form $[\mathbf{1}^{bp}\text{-CO}_2\text{CO}_2]{}^{-1,c}$ from $[\mathbf{1}\text{-CO}_2\text{CO}_2]{}^0$ are operational at -1.82 V (versus $\text{Fc}^{+/0}$), however to different extents.

Having identified the different pathways leading to $[\mathbf{1}^{bp}\text{-CO}_2\text{CO}_2]{}^{-1,c}$, we dived into the possibility of C–O bond cleavage in this intermediate. Its DFT optimized structure reveals its similarity to that of $[\mathbf{1}^{bp}\text{-CO}_2\text{CO}_2]{}^0,c$, with a relatively long C–O bond (1.45 Å) that is to be cleaved. The formation of the metallacycle also induces some strain, that further weakens the C–O bond, as evidenced by the small O–Ru–C angle of 80.0° in $[\mathbf{1}^{bp}\text{-CO}_2\text{CO}_2]{}^{-1,c}$. The transition state for C–O cleavage was located just 11.2 kcal mol $^{-1}$ above $[\mathbf{1}^{bp}\text{-CO}_2\text{CO}_2]{}^{-1,c}$, resulting in $[\mathbf{1}^{bp}(\text{CO})(\text{OCO}_2)]{}^{-1}$ at 10.4 kcal mol $^{-1}$ relative to $[\mathbf{1}\text{-CO}_2]{}^0$. Dissociation of carbonate then proceeds with an activation energy at 17.2 kcal mol $^{-1}$ relative to $[\mathbf{1}\text{-CO}_2]{}^0$, accompanied by restoration of the bidentate coordination mode of CH_3bpy to Ru to form $[\mathbf{1}\text{-CO}]{}^+$ (Figure 3). The highest activation energy barriers (ΔG^\ddagger) in the pathway (Figure 3) are for the formation of $[\mathbf{1}^{bp}\text{-CO}_2\text{CO}_2]{}^0,c$ at 17.3 kcal mol $^{-1}$ and the release of carbonate at a similar free energy (ΔG^\ddagger relative to $[\mathbf{1}\text{-CO}_2]{}^0$) of 17.2 kcal mol $^{-1}$. The barriers agree well with the experimental maximum turnover frequency (TOF_{max})^[57] of 1.8 s $^{-1}$ which corresponds to an activation free energy of 17.2 kcal mol $^{-1}$ as obtained from Eyring equation^[75] (see Supporting Information for details of this conversion).

Having identified the flexible coordination of the bidentate ligand and the subsequent formation of the $[\mathbf{1}^{bp}\text{-CO}_2\text{CO}_2]{}^{-1,c}$ metallacycle as crucial features for efficient C–O bond cleavage, focus was directed towards the 1,10-phenanthroline analogue $[\mathbf{2}\text{-CO}_2]{}^0$ (Figure 4). Analogous to $[\mathbf{1}\text{-CO}_2]{}^0$, it reacts with another CO_2 molecule to form the $[\mathbf{2}\text{-CO}_2\text{CO}_2]{}^0$ intermediate, with an activation free energy of 10.9 kcal mol $^{-1}$, the reaction free energy being 4.1 kcal mol $^{-1}$ (Figure 4).

The intramolecular cyclization in $[\mathbf{2}\text{-CO}_2\text{CO}_2]{}^0$ by the attack of the terminal oxygen of $-\text{CO}_2\text{CO}_2$ onto Ru, to produce a metallacyclic intermediate analogous to that for complex $\mathbf{1}^{2+}$ was then investigated. Since the structure of CH_3phen is more rigid than CH_3bpy as mentioned earlier, the partial decooordination of CH_3phen from $[\mathbf{2}\text{-CO}_2\text{CO}_2]{}^0$ (Figure 4) is expected to be more difficult than CH_3bpy . This is in fact the case, as the DFT optimization of the transition state (TS) for this process resulted in complete decooordination of CH_3phen from Ru (Figures S9(a) and S9(c)). The activation free energy for this process was calculated to be 22.2 kcal mol $^{-1}$ with respect to $[\mathbf{2}\text{-CO}_2]{}^0$

(Figure S9(d)), higher than the analogous activation barrier of 17.3 kcal mol $^{-1}$ for the formation of $[\mathbf{1}^{bp}\text{-CO}_2\text{CO}_2]{}^0,c$ (Figure 3). The reaction free energy of the cyclic intermediate $[\mathbf{2}^{phen}\text{-CO}_2\text{CO}_2]{}^0,c$ (Figure S9(b)) was 4.0 kcal mol $^{-1}$ (Figure S9(d)). The higher ΔG^\ddagger for the formation of $[\mathbf{2}^{phen}\text{-CO}_2\text{CO}_2]{}^0,c$ prompted us to find another pathway for the formation of a related cyclic intermediate, $[\mathbf{2}^{bp}\text{-CO}_2\text{CO}_2]{}^0,c$, achieved by liberation of one of the pyridine units of the $t\text{Bu}_3\text{tpy}$ ligand in $[\mathbf{2}\text{-CO}_2\text{CO}_2]{}^0$ instead (Figure 4). The activation free energy for this cyclization step was calculated as 12.9 kcal mol $^{-1}$, with $[\mathbf{2}^{bp}\text{-CO}_2\text{CO}_2]{}^0,c$ being merely 0.6 kcal mol $^{-1}$ lower in energy than $[\mathbf{2}\text{-CO}_2\text{CO}_2]{}^0$. The difference of 9.3 kcal mol $^{-1}$ in ΔG^\ddagger for the formation of $[\mathbf{2}^{phen}\text{-CO}_2\text{CO}_2]{}^0,c$ versus $[\mathbf{2}^{bp}\text{-CO}_2\text{CO}_2]{}^0,c$, indicates that the latter is preferred. These energies therefore show that replacement of $-\text{CH}_3\text{bpy}$ with $-\text{CH}_3\text{phen}$ has made the partial decooordination of $t\text{Bu}_3\text{tpy}$ more probable both kinetically and thermodynamically.

An interesting observation is the appreciable differences in activation free energy ($19.6\text{--}12.9=6.7$ kcal mol $^{-1}$) and free energy of formation ($4.7+0.6=5.3$ kcal mol $^{-1}$) of the metallacyclic intermediates $[\mathbf{1}^{bp}\text{-CO}_2\text{CO}_2]{}^0,c$ and $[\mathbf{2}^{bp}\text{-CO}_2\text{CO}_2]{}^0,c$, obtained by the partial decooordination of $t\text{Bu}_3\text{tpy}$ in $[\mathbf{1}\text{-CO}_2\text{CO}_2]{}^0$ and $[\mathbf{2}\text{-CO}_2\text{CO}_2]{}^0$ respectively, with $[\mathbf{1}^{bp}\text{-CO}_2\text{CO}_2]{}^0,c$ being higher in energy than $[\mathbf{1}\text{-CO}_2\text{CO}_2]{}^0$ by 4.7 kcal mol $^{-1}$, whereas $[\mathbf{2}^{bp}\text{-CO}_2\text{CO}_2]{}^0,c$ is 0.6 kcal mol $^{-1}$ lower than $[\mathbf{2}\text{-CO}_2\text{CO}_2]{}^0$ (Figure S10(a)). These energy differences may be attributed to $[\mathbf{1}\text{-CO}_2\text{CO}_2]{}^0$ being more polar than $[\mathbf{2}\text{-CO}_2\text{CO}_2]{}^0$ as seen from their electrostatic potential maps on total electron density (Figures S10(b) and S10(c)). The polarity differences arise from the fact that CH_3bpy is a better electron donor than CH_3phen .^[76] The metallacyclic intermediates are however, similar in polarity due to the negative charge on the terminal oxygen being neutralised by the cationic Ru centre (Figures S10(d) and S10(e)). As expected on grounds of the polarity of the molecule, $[\mathbf{1}\text{-CO}_2\text{CO}_2]{}^0$ is associated with a more negative solvation free energy than $[\mathbf{2}\text{-CO}_2\text{CO}_2]{}^0$ (Table S2). Therefore, the difference in solvation free energies (ΔE_{solv}) between $[\mathbf{1}\text{-CO}_2\text{CO}_2]{}^0$ and $[\mathbf{1}^{bp}\text{-CO}_2\text{CO}_2]{}^0,c$ is -27.74 kcal mol $^{-1}$, whereas between $[\mathbf{2}\text{-CO}_2\text{CO}_2]{}^0$ to $[\mathbf{2}^{bp}\text{-CO}_2\text{CO}_2]{}^0,c$ it is -23.89 kcal mol $^{-1}$ (Table S2). Hence, the difference of 3.85 kcal mol $^{-1}$ $\{(-23.89)-(-27.74)\}$, in solvation free energy change, is what contributes to the difference in reaction free energies for partial decooordination of $t\text{Bu}_3\text{tpy}$ in complexes **1** and **2**. Another minor contribution perhaps comes from the fact that CH_3bpy is more susceptible towards structural distortion than CH_3phen . This leads to slightly more distorted structure of $[\mathbf{1}^{bp}\text{-CO}_2\text{CO}_2]{}^0,c$ as compared to $[\mathbf{2}^{bp}\text{-CO}_2\text{CO}_2]{}^0,c$ (Table S3), which in turn results in better overlap of orbitals in $[\mathbf{2}^{bp}\text{-CO}_2\text{CO}_2]{}^0,c$, as seen from the highest occupied molecular orbitals (HOMO) (Figures S10(f) and S10(g)).

In analogy to the situation in $[\mathbf{1}^{bp}\text{-CO}_2\text{CO}_2]{}^0,c$, the formation of the cyclic intermediate $[\mathbf{2}^{bp}\text{-CO}_2\text{CO}_2]{}^0,c$ allows access to a further reduction at a potential of -1.80 V (versus $\text{Fc}^{+/0}$) (Figure 4) that is slightly more positive than the first reduction. The result is the three-electron reduced, cyclic adduct $[\mathbf{2}^{bp}\text{-CO}_2\text{CO}_2]{}^{-1,c}$ which is found as the lowest

energy intermediate in the catalytic pathway (Figure 4), just before C–O bond cleavage.

The further reduction of $[2\text{-CO}_2\text{CO}_2]^0$ to $[2\text{-CO}_2\text{CO}_2]^{-1}$, followed by intramolecular cyclization of the latter to form $[2^p\text{-CO}_2\text{CO}_2]^{-1,c}$ was investigated as an alternative pathway (Figure S11). The reduction event was calculated to occur at -2.15 V (versus $\text{Fc}^{+/0}$), 330 mV more negative than the applied potential of -1.82 V (versus $\text{Fc}^{+/0}$). The cyclization of $[2\text{-CO}_2\text{CO}_2]^{-1}$ to $[2^p\text{-CO}_2\text{CO}_2]^{-1,c}$ then proceeds with an activation free energy of 12.1 kcal mol $^{-1}$, which is merely 0.9 kcal mol $^{-1}$ lower than the ΔG^\ddagger of 13.0 kcal mol $^{-1}$ for the conversion of $[2\text{-CO}_2\text{CO}_2]^0$ to $[2^p\text{-CO}_2\text{CO}_2]^{0,c}$ (Figure S11). These energies combined with the 330 mV difference in potentials result in an estimated apparent rate of this alternative pathway to be around seven orders of magnitude lower than that incorporating the intramolecular cyclization of $[2\text{-CO}_2\text{CO}_2]^0$ followed by reduction (details of calculation under Figure S11). This striking difference in apparent rates rules out the pathway that passes through the reduction of $[2\text{-CO}_2\text{CO}_2]^0$ to $[2\text{-CO}_2\text{CO}_2]^{-1}$.

The relatively high computed stabilities of the cyclic intermediates $[1^{bp}\text{-CO}_2\text{CO}_2]^{-1,c}$, $[2^p\text{-CO}_2\text{CO}_2]^{0,c}$ and $[2^p\text{-CO}_2\text{CO}_2]^{-1,c}$ indicate that their spectroscopic observation during electrocatalytic CO_2 reduction might be feasible. Hence, we resorted to infra-red (IR) spectroscopy. Experimentally, the relevant region in the infra-red (IR) spectra is convoluted by the evolution of three major bands at 1684 cm $^{-1}$, 1645 cm $^{-1}$ and 1304 cm $^{-1}$ that arise from the reductive disproportionation product CO_3^{2-} (Figures 5a and S12(a)); peaks are marked by asterisks *), as previously reported for 1^{2+} .^[56,79] Similar spectral features are also observed in the experimental FT-IR spectra obtained from 2^{2+} in the current study (Figures 5b and S12(b)).

A close inspection of the FT-IR spectra obtained during the controlled potential electrolysis (CPE) of a 1.0 mM solution of 1^{2+} in anhydrous CH_3CN under CO_2 (0.28 M) (Figure 5a) reveals the evolution of a weak shoulder at 1740 cm $^{-1}$ along with some convoluted transitions near 1230 cm $^{-1}$.^[56] DFT calculations show that these two absorptions most likely arise from a symmetric and an asymmetric C=O stretching vibration (Figure S13(c)) that are however ambiguous to assign to one particular species.^[78] Both $[1\text{-CO}_2]^0$ (calc. at 1731 cm $^{-1}$ and 1235 cm $^{-1}$; Figures S13(a)) and $[1^{bp}\text{-CO}_2\text{CO}_2]^{-1,c}$ (calc. at 1759 cm $^{-1}$ and 1235 cm $^{-1}$; Figure S13(b)) exhibit calculated IR vibrations that correspond well with the experimentally observed ones.

Furthermore, IR bands were observed at 2001 , 1960 and 1932 cm $^{-1}$ during CPE of 1^{2+} (Figure S14) and at 2086 , 2001 and 1932 cm $^{-1}$ during CPE of 2^{2+} (Figure S15) in anhydrous CH_3CN under CO_2 (0.28 M). These bands correspond very well with the DFT calculated IR spectral transitions at 2004 , 1954 and 1925 cm $^{-1}$ for $[1\text{-CO}]^{2+}$, $[1\text{-CO}]^+$, $[1\text{-CO}]^0$ respectively (Figure S16), and at 2078 , 2007 , and 1925 cm $^{-1}$ for $[2\text{-CO}]^{2+}$, $[2\text{-CO}]^+$, $[2\text{-CO}]^0$ respectively (Figure S17). We were also able to observe the growth of the band for free CO in CH_3CN at 2140 cm $^{-1}$ during CPE of 2^{2+} (Figures S15(b) and S15(c)).

IR spectra recorded during the CPE of 2^{2+} at -1.82 V (versus $\text{Fc}^{+/0}$) under CO_2 (0.28 M) display the evolution of

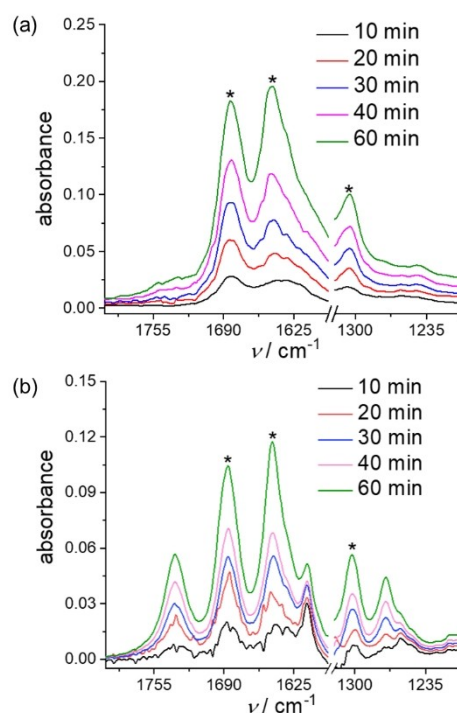


Figure 5. Fourier transformed infra-red (FT-IR) absorbance spectra of aliquots taken during controlled potential electrolysis of CO_2 saturated (0.28 M) solutions of (a) $1(\text{PF}_6)_2$ (1.0 mM) and (b) $2(\text{PF}_6)_2$ (1.0 mM), in anhydrous $\text{CH}_3\text{CN}/0.1$ M TBAPF $_6$ at an applied potential of -1.82 V (versus $\text{Fc}^{+/0}$). The peaks marked with * arise from the CO_3^{2-} .

clearly visible bands at 1735 , 1612 and 1272 cm $^{-1}$ along with those of the CO_3^{2-} byproduct (Figures 5b and S12(b)). The 1735 cm $^{-1}$ band can be explained by a C=O stretching vibration in either $[2\text{-CO}_2]^0$ or $[2^p\text{-CO}_2\text{CO}_2]^{0,c}$; (calc: 1729 cm $^{-1}$ and 1760 cm $^{-1}$, respectively; Figures S18(a) and S18(c)), while no absorption is expected for $[2^p\text{-CO}_2\text{CO}_2]^{-1,c}$ in this range according to its DFT calculated IR spectrum (Figures S18(d)). The experimental IR band at 1272 cm $^{-1}$ corresponds very well to computed C–O stretches at 1253 cm $^{-1}$ and 1291 cm $^{-1}$ for $[2^p\text{-CO}_2\text{CO}_2]^{0,c}$ and $[2^p\text{-CO}_2\text{CO}_2]^{-1,c}$ respectively (Figures S18(c) and S18(d)^[79]), while the experimentally obtained peak at 1612 cm $^{-1}$ is only found in the calculated IR spectrum of $[2^p\text{-CO}_2\text{CO}_2]^{-1,c}$ at 1614 cm $^{-1}$ (Figures 5b and S18(d)). This unique absorption allows for the identification of $[2^p\text{-CO}_2\text{CO}_2]^{-1,c}$ as one of the intermediates accumulated during CPE. Thus, the IR monitoring indicates the presence of $[2\text{-CO}_2]^0$, $[2^p\text{-CO}_2\text{CO}_2]^{0,c}$ and $[2^p\text{-CO}_2\text{CO}_2]^{-1,c}$ being built up during CPE, consistent with the small calculated energy differences between these intermediates (3.5 kcal mol $^{-1}$ between $[2\text{-CO}_2]^0$ and $[2^p\text{-CO}_2\text{CO}_2]^{0,c}$; 3.0 kcal mol $^{-1}$ between $[2\text{-CO}_2]^0$ and $[2^p\text{-CO}_2\text{CO}_2]^{-1,c}$; Figure 4). Linear $[2\text{-CO}_2\text{CO}_2]^0$ is not present in detectable amounts, as its diagnostic calculated IR absorption at 1869 cm $^{-1}$ (Figure S18(b)) is absent from the experimental CPE monitoring (Figure S19).

Conducting CPE of 2^{2+} under identical conditions, but with $^{13}\text{CO}_2$ gives rise to FT-IR spectra that are qualitatively similar to the ones under $^{12}\text{CO}_2$, with the expected shifts due

to the isotope labelling. The C=O and C–O stretching vibrations shift by 40–50 and 15–20 cm^{−1} to lower wavenumbers,^[78] respectively, when going from ¹²CO₂ to ¹³CO₂,^[55,64] confirming that these IR bands arise from CO₂-derived species (Figure S20). The calculated IR bands of [^{2p}-¹³CO₂¹³CO₂]^{−1,c} agree well with the experimentally observed ones from CPE (ν (cm^{−1}): experimental (calc.): 1642 (1648), 1564 (1575) and 1279 (1265) cm^{−1}, Figures S20 and S21).

The IR-spectroscopic observation of [^{2p}-CO₂CO₂]^{−1,c} is consistent with a lower rate of C–O bond dissociation compared to that in [^{1bp}-CO₂CO₂]^{−1,c} as evidenced by a higher DFT calculated activation free energy (16.6 kcal mol^{−1} for [^{2p}-CO₂CO₂]^{−1,c} versus 11.2 kcal mol^{−1} for [^{1bp}-CO₂CO₂]^{−1,c}; Figures 3 and 4).

The highest activation energy barriers (ΔG^\ddagger) in the pathway for **2**²⁺ (Figure 4) relative to [**2**-CO₂]⁰ are associated with the cleavage of C–O bond in [^{2p}-CO₂CO₂]^{−1,c} at 19.6 kcal mol^{−1} and the release of CO₃^{2−} at 19.1 kcal mol^{−1}. The barriers correspond quite well with the experimental catalytic rate constant k_{cat} (or maximum turnover frequency (TOF_{max})) of 0.85 s^{−1}, obtained using Foot-Of-the-Wave-Analysis (FOWA)^[80,81] (Figures S22(a) and S22(b); see Supporting Information for details). The rate constant of 0.85 s^{−1} translates to a free energy barrier of 17.5 kcal mol^{−1} (calculated using the Eyring equation^[76] as described earlier for **1**²⁺), which differs from the DFT calculated barrier by merely 2.1 kcal mol^{−1}. Therefore, the trend in the experimental catalytic rates of **1**²⁺ > **2**²⁺ agree very well with the corresponding trends in their DFT calculated activation barriers (Figures 3 and 4). The deduction of k_{cat} allowed us to construct the Tafel plots of log(TOF) versus overpotential (η) (Figure S22(c)) for **1**²⁺ and **2**²⁺. This provided log(TOF_0) (TOF_0 =turnover frequency at zero overpotential) as −7.64 s^{−1} and −8.20 s^{−1} for **1**²⁺^[57] and **2**²⁺ respectively.

The metallacyclic intermediate proposed in the current study is further supported by comparison with the reported IR spectrum of complex [Ir(PMe₃)₃(Cl)(COOCOO)]^[65] (Figure S7), which possesses a similar metallacycle consisting of two CO₂ molecules in a “head-to-tail” arrangement.^[65] This reference complex was prepared by the stoichiometric reaction of a low-valent metal precursor and CO₂, and exhibited IR bands at 1725, 1680, 1648 (sh), 1605, and 1290 cm^{−1},^[65] which are almost identical to the IR signature of [^{2p}-CO₂CO₂]^{−1,c} (Figures 5b and S18(d)).

Conclusion

In summary, the present work describes an unexplored mechanistic pathway for low-energy C–O bond cleavage in the reductive disproportionation of CO₂ to CO and CO₃^{2−}. Computational work in conjunction with IR spectroscopic detection of accumulated reaction intermediates established the involvement of an unprecedented 5-membered metallacyclic intermediate in the catalytic cycle, after ruling out alternative pathways. The formation of the metallacycle is enabled by the flexible ligation of the polypyridyl ligands, and it is shown that the ligand with the least binding strength

to the metal is the one that partially de-coordinates to liberate the coordination site required for metallacycle formation.

The Ru center plays a dual role in the catalytic cycle: it acts as a Lewis base and attacks the first CO₂ molecule at an early stage of the cycle, while also acting as an intramolecular Lewis acidic site to stabilize the negative charge of the [**Ru**-CO₂CO₂]⁰, thereby leading to the cyclic [**Ru**-CO₂CO₂]^{0,c}. The latter intermediate is crucial for energy-conserving turnover, as it allows for a third reduction at a more positive potential than that of the starting complexes **1**²⁺ and **2**²⁺. The thereby produced [**Ru**-CO₂CO₂]^{−1,c} contains structural features that allow for relatively facile C–O bond cleavage with the calculated activation barrier for this step being dramatically decreased as compared to that required for C–O bond cleavage in the non-cyclic [**Ru**-CO₂CO₂]⁰. Subsequent release of products closes the catalytic cycle, and gives the catalyst a good overall stability.

Considering its simplicity, it may well be that similar species in other mononuclear catalysts have hitherto been overlooked. At the same time, its identification and operation offer a new design feature that can now be implemented consciously in future catalyst designs.

Acknowledgements

The authors would like to acknowledge the Swedish National Infrastructure for Computing (SNIC), which is funded by the Swedish Research Council (VR) through grant agreement no. 2016–07213, in Linköping (NSC), for the computational resources. The computations were performed under project numbers SNIC2017/1–13, SNIC2018/3–1, SNIC2019/3–6, SNIC2020/5–41, and NAISS2023–22–89. We acknowledge NordForsk foundation (No. 85378) for the Nordic University hub NordCO₂. MA has been supported by the Swedish Research Council (VR) grant number 2018–05396, and the Knut & Alice Wallenberg (KAW) project CATSS (KAW 2016.0072). XC acknowledges the China Scholarship Council (CSC). HA and SO acknowledge the Swedish Energy Agency (grant number: 42029-1) for financial support. HA acknowledges the Cleve, Gahn and Svanberg funds from Uppsala University, Sweden, for financing the upgrading of Fourier-Transformed-Infrared-Spectrometer (FTIR) for spectroelectrochemistry. HA also acknowledges Technical University of Munich (TUM) for providing the necessary resources to finish the research work. Open Access funding enabled and organized by Projekt DEAL.

Conflict of Interest

The authors declare no conflict of interest.

Data Availability StatementReferences

The data that support the findings of this study are available in the supplementary material of this article.

Keywords: CO₂ Reduction · Electrocatalysis · Metallacyclic Intermediates · Overpotential · Polypyridyl Ligands

- [1] C. Costentin, S. Drouet, M. Robert, J.-M. Savéant, *J. Am. Chem. Soc.* **2012**, *134*, 11235–11242.
- [2] I. Azcarate, C. Costentin, M. Robert, J.-M. Savéant, *J. Am. Chem. Soc.* **2016**, *138*, 16639–16644.
- [3] C. Costentin, S. Drouet, M. Robert, J.-M. Savéant, *Science* **2012**, *338*, 90–94.
- [4] R. Francke, B. Schille, M. Roemelt, *Chem. Rev.* **2018**, *118*, 4631–4701.
- [5] F. Franco, M. F. Pinto, B. Royo, J. Lloret-Fillol, *Angew. Chem. Int. Ed.* **2018**, *57*, 4603–4606; *Angew. Chem.* **2018**, *130*, 4693–4696.
- [6] S. Fernández, F. Franco, C. Casadevall, V. Martín-Diaconescu, J. M. Luis, J. Lloret-Fillol, *J. Am. Chem. Soc.* **2020**, *142*, 120–133.
- [7] M. L. Clark, P. L. Cheung, M. Lessio, E. A. Carter, C. P. Kubiak, *ACS Catal.* **2018**, *8*, 2021–2029.
- [8] B. Merillas, E. Cuéllar, A. Díez-Varga, T. Torroba, G. García-Herbosa, S. Fernández, J. Lloret-Fillol, J. M. Martín-Alvarez, D. Miguel, F. Villafañe, *Inorg. Chem.* **2020**, *59*, 11152–11165.
- [9] P. Gerschel, A. L. Cordes, S. Bimmermann, D. Siegmund, N. Metzler-Nolte, U.-P. Apfel, *Z. Anorg. Allg. Chem.* **2021**, *647*, 968–977.
- [10] S. Sung, D. Kumar, M. Gil-Sepulcre, M. Nippe, *J. Am. Chem. Soc.* **2017**, *139*, 13993–13996.
- [11] M. Merrouch, M. Benvenuti, M. Lorenzi, C. Léger, V. Fourmond, S. Dementin, *JBIC J. Biol. Inorg. Chem.* **2018**, *23*, 613–620.
- [12] H. Dobbek, V. Svetlitchnyi, L. Gremer, R. Huber, O. Meyer, *Science* **2001**, *293*, 1281–1285.
- [13] M. Can, F. A. Armstrong, S. W. Ragsdale, *Chem. Rev.* **2014**, *114*, 4149–4174.
- [14] N. Elgrishi, M. B. Chambers, X. Wang, M. Fontecave, *Chem. Soc. Rev.* **2017**, *46*, 761–796.
- [15] S. Dey, T. K. Todorova, M. Fontecave, V. Mougél, *Angew. Chem. Int. Ed.* **2020**, *59*, 15726–15733; *Angew. Chem.* **2020**, *132*, 15856–15863.
- [16] M. E. Ahmed, A. Rana, R. Saha, S. Dey, A. Dey, *Inorg. Chem.* **2020**, *59*, 5292–5302.
- [17] E. Boutin, L. Merakeb, B. Ma, B. Boudy, M. Wang, J. Bonin, E. Anxolabéhère-Mallart, M. Robert, *Chem. Soc. Rev.* **2020**, *49*, 5772–5809.
- [18] T. Fogeron, T. K. Todorova, J.-P. Porcher, M. Gomez-Mingot, L.-M. Chamoreau, C. Mellot-Draznieks, Y. Li, M. Fontecave, *ACS Catal.* **2018**, *8*, 2030–2038.
- [19] T. Fogeron, P. Retailleau, M. Gomez-Mingot, Y. Li, M. Fontecave, *Organometallics* **2019**, *38*, 1344–1350.
- [20] A. Mouchfiq, T. K. Todorova, S. Dey, M. Fontecave, V. Mougél, *Chem. Sci.* **2020**, *11*, 5503–5510.
- [21] S. Gonell, J. Lloret-Fillol, A. J. M. Miller, *ACS Catal.* **2021**, *11*, 615–626.
- [22] S. Gonell, M. D. Massey, I. P. Moseley, C. K. Schauer, J. T. Muckerman, A. J. M. Miller, *J. Am. Chem. Soc.* **2019**, *141*, 6658–6671.
- [23] S. Gonell, E. A. Assaf, K. D. Duffee, C. K. Schauer, A. J. M. Miller, *J. Am. Chem. Soc.* **2020**, *142*, 8980–8999.
- [24] S. L. Hooe, J. M. Dressel, D. A. Dickie, C. W. Machan, *ACS Catal.* **2020**, *10*, 1146–1151.
- [25] S. L. Hooe, J. J. Moreno, A. G. Reid, E. N. Cook, C. W. Machan, *Angew. Chem. Int. Ed.* **2022**, *61*, e202109645; *Angew. Chem.* **2022**, *134*, e202109645.
- [26] A. W. Nichols, S. Chatterjee, M. Sabat, C. W. Machan, *Inorg. Chem.* **2018**, *57*, 2111–2121.
- [27] J. J. Moreno, S. L. Hooe, C. W. Machan, *Inorg. Chem.* **2021**, *60*, 3635–3650.
- [28] R. Bonetto, R. Altieri, M. Tagliapietra, A. Barbon, M. Bonchio, M. Robert, A. Sartorel, *ChemSusChem* **2020**, *13*, 4111–4120.
- [29] L. Rotundo, C. Garino, E. Priola, D. Sassone, H. Rao, B. Ma, M. Robert, J. Fiedler, R. Gobetto, C. Nervi, *Organometallics* **2019**, *38*, 1351–1360.
- [30] C. Cometto, L. Chen, E. Anxolabéhère-Mallart, C. Fave, T.-C. Lau, M. Robert, *Organometallics* **2019**, *38*, 1280–1285.
- [31] C. Cometto, L. Chen, P.-K. Lo, Z. Guo, K.-C. Lau, E. Anxolabéhère-Mallart, C. Fave, T.-C. Lau, M. Robert, *ACS Catal.* **2018**, *8*, 3411–3417.
- [32] A. Maurin, C.-O. Ng, L. Chen, T.-C. Lau, M. Robert, C.-C. Ko, *Dalton Trans.* **2016**, *45*, 14524–14529.
- [33] L. Chen, Z. Guo, X.-G. Wei, C. Gallenkamp, J. Bonin, E. Anxolabéhère-Mallart, K.-C. Lau, T.-C. Lau, M. Robert, *J. Am. Chem. Soc.* **2015**, *137*, 10918–10921.
- [34] C. Costentin, M. Robert, J.-M. Savéant, A. Tatin, *Proc. Natl. Acad. Sci. USA* **2015**, *112*, 6882–6886.
- [35] C. Costentin, G. Passard, M. Robert, J.-M. Savéant, *J. Am. Chem. Soc.* **2014**, *136*, 11821–11829.
- [36] N. Queyriaux, K. Abel, J. Fize, J. Pécaut, M. Orio, L. Hammarström, *Sustainable Energy Fuels* **2020**, *4*, 3668–3676.
- [37] F. Franco, C. Cometto, L. Nencini, C. Barolo, F. Sordello, C. Minero, J. Fiedler, M. Robert, R. Gobetto, C. Nervi, *Chem. Eur. J.* **2017**, *23*, 4782–4793.
- [38] K. T. Ngo, M. McKinnon, B. Mahanti, R. Narayanan, D. C. Grills, M. Z. Ertem, J. Rochford, *J. Am. Chem. Soc.* **2017**, *139*, 2604–2618.
- [39] J. Agarwal, T. W. Shaw, H. F. Schaefer, A. B. Bocarsly, *Inorg. Chem.* **2015**, *54*, 5285–5294.
- [40] S. E. Tignor, T. W. Shaw, A. B. Bocarsly, *Dalton Trans.* **2019**, *48*, 12730–12737.
- [41] P. Gotico, L. Roupnel, R. Guillot, M. Sircoglou, W. Leibl, Z. Halime, A. Aukauloo, *Angew. Chem. Int. Ed.* **2020**, *59*, 22451–22455; *Angew. Chem.* **2020**, *132*, 22637–22641.
- [42] J. A. Buss, D. G. VanderVelde, T. Agapie, *J. Am. Chem. Soc.* **2018**, *140*, 10121–10125.
- [43] P. Sen, B. Mondal, D. Saha, A. Rana, A. Dey, *Dalton Trans.* **2019**, *48*, 5965–5977.
- [44] D. Z. Zee, M. Nippe, A. E. King, C. J. Chang, J. R. Long, *Inorg. Chem.* **2020**, *59*, 5206–5217.
- [45] M. Loipersberger, D. Z. Zee, J. A. Panetier, C. J. Chang, J. R. Long, M. Head-Gordon, *Inorg. Chem.* **2020**, *59*, 8146–8160.
- [46] M. H. Rønne, D. Cho, M. R. Madsen, J. B. Jakobsen, S. Eom, É. Escoudé, H. C. D. Hammershøj, D. U. Nielsen, S. U. Pedersen, M.-H. Baik, T. Skrydstrup, K. Daasbjerg, *J. Am. Chem. Soc.* **2020**, *142*, 4265–4275.
- [47] C. G. Margarit, C. Schnedermann, N. G. Asimow, D. G. Nocera, *Organometallics* **2019**, *38*, 1219–1223.
- [48] M. R. Madsen, J. B. Jakobsen, M. H. Rønne, H. Liang, H. C. D. Hammershøj, P. Nørby, S. U. Pedersen, T. Skrydstrup, K. Daasbjerg, *Organometallics* **2020**, *39*, 1480–1490.
- [49] S. Amanullah, P. Saha, A. Nayek, M. E. Ahmed, A. Dey, *Chem. Soc. Rev.* **2021**, *50*, 3755–3823.
- [50] S. Roy, B. Sharma, J. Pécaut, P. Simon, M. Fontecave, P. D. Tran, E. Derat, V. Artero, *J. Am. Chem. Soc.* **2017**, *139*, 3685–3696.
- [51] E. Haviv, D. Azaiza-Dabbah, R. Carmieli, L. Avram, J. M. L. Martin, R. Neumann, *J. Am. Chem. Soc.* **2018**, *140*, 12451–12456.

- [52] S. Sung, X. Li, L. M. Wolf, J. R. Meeder, N. S. Bhuvanesh, K. A. Grice, J. A. Panetier, M. Nippe, *J. Am. Chem. Soc.* **2019**, *141*, 6569–6582.
- [53] M. Hammouche, D. Lexa, M. Momenteau, J. M. Saveant, *J. Am. Chem. Soc.* **1991**, *113*, 8455–8466.
- [54] I. Bhugun, D. Lexa, J.-M. Savéant, *J. Phys. Chem.* **1996**, *100*, 19981–19985.
- [55] M. D. Sampson, C. P. Kubiak, *J. Am. Chem. Soc.* **2016**, *138*, 1386–1393.
- [56] B. A. Johnson, S. Maji, H. Agarwala, T. A. White, E. Mijangos, S. Ott, *Angew. Chem. Int. Ed.* **2016**, *55*, 1825–1829; *Angew. Chem.* **2016**, *128*, 1857–1861.
- [57] B. A. Johnson, H. Agarwala, T. A. White, E. Mijangos, S. Maji, S. Ott, *Chem. Eur. J.* **2016**, *22*, 14870–14880.
- [58] S. Nishigaki, H. Yoshioka, K. Nakatsu, *Acta Crystallogr. Sect. B* **1978**, *34*, 875–879.
- [59] L. L. Merritt, E. Schroeder, *Acta Crystallogr.* **1956**, *9*, 801–804.
- [60] A. Gennaro, A. A. Isse, E. Vianello, *J. Electroanal. Chem. Interfacial Electrochem.* **1990**, *289*, 203–215.
- [61] Z. Chen, C. Chen, D. R. Weinberg, P. Kang, J. J. Concepcion, D. P. Harrison, M. S. Brookhart, T. J. Meyer, *Chem. Commun.* **2011**, *47*, 12607–12609.
- [62] J. Agarwal, E. Fujita, H. F. Schaefer, J. T. Muckerman, *J. Am. Chem. Soc.* **2012**, *134*, 5180–5186.
- [63] B. P. Sullivan, C. M. Bolinger, D. Conrad, W. J. Vining, T. J. Meyer, *J. Chem. Soc. Chem. Commun.* **1985**, 1414–1416.
- [64] C. W. Machan, S. A. Chabolla, J. Yin, M. K. Gilson, F. A. Tezcan, C. P. Kubiak, *J. Am. Chem. Soc.* **2014**, *136*, 14598–14607.
- [65] T. Herskovitz, L. J. Guggenberger, *J. Am. Chem. Soc.* **1976**, *98*, 1615–1616.
- [66] P. M. Jurd, H. L. Li, M. Bhadbhade, L. D. Field, *Organometallics* **2020**, *39*, 2011–2018.
- [67] M. Feller, U. Gellrich, A. Anaby, Y. Diskin-Posner, D. Milstein, *J. Am. Chem. Soc.* **2016**, *138*, 6445–6454.
- [68] J. Langer, W. Imhof, M. J. Fabra, P. García-Orduña, H. Görls, F. J. Lahoz, L. A. Oro, M. Westerhausen, *Organometallics* **2010**, *29*, 1642–1651.
- [69] R. Kempe, J. Sieler, D. Walther, J. Reinhold, K. Rommel, Z. Anorg. Allg. Chem. **1993**, *619*, 1105–1110.
- [70] L. Dahlenburg, C. Prengel, *J. Organomet. Chem.* **1986**, *308*, 63–71.
- [71] E. Carmona, F. Gonzalez, M. L. Poveda, J. M. Marin, J. L. Atwood, R. D. Rogers, *J. Am. Chem. Soc.* **1983**, *105*, 3365–3366.
- [72] F. Lucarini, J. Fize, A. Morozan, M. Marazzi, M. Natali, M. Pastore, V. Artero, A. Ruggi, *Sustainable Energy Fuels* **2020**, *4*, 589–599.
- [73] J. J. Leung, J. Warnan, K. H. Ly, N. Heidary, D. H. Nam, M. F. Kuehnle, E. Reisner, *Nat. Catal.* **2019**, *2*, 354–365.
- [74] S. Aroua, T. K. Todorova, V. Mougél, P. Hommes, H.-U. Reissig, M. Fontecave, *ChemCatChem* **2017**, *9*, 2099–2105.
- [75] H. Eyring, *Chem. Rev.* **1935**, *17*, 65–77.
- [76] Q. Teng, H. V. Huynh, *Inorg. Chem.* **2014**, *53*, 10964–10973.
- [77] S. C. Cheng, C. A. Blaine, M. G. Hill, K. R. Mann, *Inorg. Chem.* **1996**, *35*, 7704–7708.
- [78] C. Jegat, M. Fouassier, M. Tranquille, J. Mascetti, I. Tommasi, M. Aresta, F. Ingold, A. Dedieu, *Inorg. Chem.* **1993**, *32*, 1279–1289.
- [79] The remaining calculated peaks at 1695 cm⁻¹ and 1291 cm⁻¹ for [2-CO₂CO₂]^{-1,c} are masked by the CO₃²⁻/HCO₃²⁻ IR bands centered at 1686 cm⁻¹ and 1301 cm⁻¹.
- [80] V. C. C. Wang, B. A. Johnson, *ACS Catal.* **2019**, *9*, 7109–7123.
- [81] C. Costentin, J.-M. Savéant, *ChemElectroChem* **2014**, *1*, 1226–1236.

Manuscript received: December 19, 2022

Accepted manuscript online: February 17, 2023

Version of record online: March 10, 2023